Analysis of the Impact of Variable Speed Limits on Environmental Sustainability and Traffic Performance in Urban Networks

Bassel Othman, Giovanni De Nunzio, Domenico Di Domenico, Carlos Canudas de Wit

Analysis of the impact of variable speed limits on environmental sustainability and traffic performance in urban networks

Bassel Othman, Giovanni De Nunzio, Domenico Di Domenico, and Carlos Canudas-de-Wit

***Abstract*—This work focuses on evaluating the potential of variable speed limits (VSLs) in a synthetic urban network to improve both environmental sustainability and traffic performance. The traffic system is modeled using the microscopic traffic simulator SUMO, and a physical fuel consumption and NOx emission model is used to assess the vehicles' energy efficiency. Speed limits are controlled through a nonlinear model predictive control (NMPC) approach, in which the traffic evolution and fuel consumption are respectively predicted with a macroscopic traffic model, namely the cell transmission model (CTM), and a pre-calibrated artificial neural network (ANN). The results reveal that in transient phases between different levels of congestion, the proposed eco-VSL controller is faster to decongest the network, resulting in an improvement of the environmental sustainability and the traffic performance both in the controlled network, and at its boundary roads.**

***Index Terms*—Variable Speed Limits, Energy efficiency, Pollutant emissions, Traffic modeling, Model Predictive Control, Artificial Neural Networks**

I. Introduction

The current acceleration of environmental degradations is partly due to the transportation sector. In cities, pollutant emissions are of particular concern as they have been associated with an increased rate of death from cardiovascular and respiratory causes [1], [2]. Authorities seek innovative approaches to address these environmental and health issues. One lever is traffic eco-management, i.e. the dynamic control of vehicles and/or urban infrastructures to reduce air pollution [3]. The benefits of traffic management approaches on the environmental sustainability can be greatly increased thanks to the technological resources offered by connected and automated vehicles (CAVs). They widen the scope of possibilities in terms of rerouting, green priority, speed advice at intersections, cooperative control, vehicle platooning, etc. [4], [5].

Vehicles' control consists mainly in strategies of eco-driving, i.e. computing a vehicle speed trajectory that minimizes emissions and energy consumption along a given route, and eco-routing, i.e. planning a minimum energy and emissions route [6]–[8]. The control of infrastructures corresponds essentially to ramp metering [9], [10], traffic light signals (TLS) control [11]–[13], and variable speed limits (VSLs). The effect of lower constant speed limits on energy efficiency has been investigated in the literature [14], [15]. VSLs go further and dynamically adapt speed limits to traffic conditions in order to resolve traffic breakdown, and improve safety, traffic throughput, and environmental sustainability. They are based on reinforcement learning [16], receding horizon optimization [17], etc. VSLs have been largely investigated in highways [18], [19], and some of these works focus on the ecological aspect of the problem [20]–[22]. However, these approaches are much less common in urban networks [17], [23], [24], especially when considering energy efficiency optimization [25]–[27].

It is essential to keep in mind that the potential of VSLs has been questioned in the literature because of bottlenecks, weaving sections, on/off ramps, lane drops, drivers prone to traffic violation, etc. [28], especially since the the impact of VSLs on traffic has not been sufficiently analyzed with real data [29].

This study presents an eco-VSL controller aimed at improving the environmental sustainability as well as the fluidity of road traffic in an urban environment. A synthetic urban network with signalized intersections and regulated turning movements is used. We assume that vehicles have real time access to the speed limits through adaptive traffic signs or Infrastructure-to-Vehicle (I2V) communication. Also, each vehicle is considered to be scrupulously respectful of speed limits.

In this work, traffic is modeled using the microscopic simulator SUMO, and a nonlinear model predictive control (NMPC) framework is implemented to regulate speed limits in the network. The eco-VSL controller predicts the evolution of traffic in the microscopic simulator with a macroscopic traffic model, namely the cell transmission model (CTM), adapted to the urban environment. Similarly, a macroscopic energy model based on an artificial neural network (ANN) is calibrated in order to predict fuel consumption levels. Finally, a microscopic physical energy model is introduced to evaluate the traffic energy efficiency and NOx emissions level. Different scenarios are analyzed to evaluate the behavior of the controller under various traffic situations. Its performance is evaluated by comparing the resulting traffic situation with baseline 30 km/h and 50 km/h speed limits simulations.

The contributions of this paper are summarized as follows:

- This study proposes a VSL control strategy in an urban

Bassel Othman and Giovanni De Nunzio are with IFP Energies nouvelles, Rond-point de l'échangeur de Solaize, BP 3, 69360 Solaize, France (e-mail: bassel.othman@ifpen.fr; giovanni.de-nunzio@ifpen.fr).

Domenico Di Domenico is with TotalEnergies SE, 12 Allée du Levant, 69890 La tour de Salvagny, France (e-mail: domenico.di-domenico@totalenergies.com).

Carlos Canudas-de-Wit is with the GIPSA-Laboratory, CNRS, Inria, Grenoble INP, Université Grenoble Alpes, 38000 Grenoble, France (e-mail: carlos.canudas-de-wit@gipsa-lab.fr).

road network with a direct consideration of the effects of control outside the controlled area.
- Relevant microscopic and macroscopic traffic models have been adapted to the needs of the study and calibrated using real-world driving data.
- An ANN adapted to the proposed strategy has been calibrated to approximate the results of the microscopic energy model.
- To the best of our knowledge, the potential of large-scale VSLs in an urban environment with explicit ecological considerations has not been investigated in the literature.

The body of this paper is organized as follows. Section II presents the traffic models used in the microscopic simulator and for the macroscopic traffic prediction. The fuel consumption and NOx emission models are introduced in Section III. The online VSL control strategy is described in Section IV, and its performance is analyzed in Section V. Finally, Section VI contains concluding remarks and a discussion on future perspectives.

II. Traffic models

This section presents the microscopic traffic model considered in the system, as well as the macroscopic one used for prediction purposes.

A. Microscopic traffic model

The plant dynamics is governed by the microscopic car-following intelligent driver model (IDM) introduced in [30], which is one of the most reliable microscopic traffic models [31]. All simulations are performed in the open source traffic simulator SUMO [32]. The drivers' decision to accelerate or to brake depends on their own speed and on the position and speed of the leading vehicle immediately ahead. We assume that all vehicles are identical, and their length is denoted l_{veh}. The model notations are illustrated in Fig. 1.

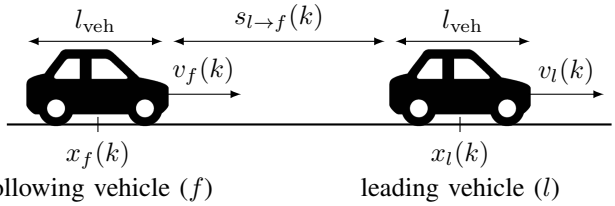

Fig. 1: Representation of the car-following model paramaters.

At time step k, the IDM calculates the acceleration $a_f(k)$ of a following vehicle f in position $x_f(k)$ traveling at speed $v_f(k)$ behind a leading vehicle l in $x_l(k)$ traveling at $v_l(k)$, using the following ordinary differential equation

$$a_f(k) = a\left[1 - \left(\frac{v_f(k)}{v_0}\right)^{\delta} - \left(\frac{s^*_{l\to f}(k)}{s_{l\to f}(k)}\right)^2\right] \quad (1)$$

where δ_t, δ, and v_0 are respectively the time step duration, the acceleration exponent, and the desired speed. The variables $s_{l\to f}(k)$ and $s^*_{l\to f}(k)$ denote respectively the current and desired distance between vehicles l and f, defined as

$$s^{\text{veh}}(k) = x^{\text{veh}}_{p-1}(k) - x^{\text{veh}}_{p}(k) - l_{\text{veh}} \quad (2)$$

$$s^*_{l\to f}(k) = s_0 + \max\left\{0, hv_f(k) + \frac{v_f(k)\Delta v_{l\to f}(k)}{2\sqrt{ab}}\right\} \quad (3)$$

where $\Delta v_{l\to f}(k)$ is the speed difference between vehicles f and l. Parameters s_0, h, a, and b denote respectively the minimum gap at complete standstill, the time headway, the maximum acceleration, and the comfortable deceleration. Their calibration is detailed in [33] and the values obtained are given in Table I.

Symbol	Description	Value	Unit
a	Maximum acceleration	2.4	m/s^2
b	Comfortable deceleration	2.8	m/s^2
s_0	Minimum distance between vehicles	2	m
v_0	Desired speed (control variable)	u	m/s
δ	Acceleration exponent	4	–
h	Time headway	1	s

TABLE I: IDM calibrated parameters.

B. Macroscopic traffic model

Due to their reduced computational burden, macroscopic traffic models are useful for predicting traffic evolution. However, they do not capture all traffic disruptions, such as stop-and-go waves or traffic breakdowns that result from drivers' behavior [25]. Among them, higher-order models are the most precise under certain traffic conditions, such as jam waves [34], and they estimate the average traffic speed more precisely. However, they are more complex, and first-order models are generally sufficient in urban environments as nonlinear flow dynamics are of less importance because of intersections and TLS [35]. As a result, first-order models have been widely used for traffic control applications in urban areas [3].

In this work, the CTM [36] is used as it is one of the most prevalent first-order traffic models. Also, cells of the same length simplify the energy consumption estimation. The CTM is extended to urban networks by considering TLS, and the First In, First Out (FIFO) policy at intersections.

1) Network characterization: In order to run the CTM in an urban network, it is essential to accurately characterize the network connections, the drivers' behavior at intersections, and the operation of TLS.

We consider an urban road network composed of one-way roads, each road being divided into several cells of same length δ_x. The set of all cells that constitute the network is denoted $\mathcal{R}$. To characterize the connections between cells, each cell $i \in \mathcal{R}$ is associated with two sets $\mathcal{P}_i$ and $\mathcal{N}_i$ containing respectively the upstream and the downstream cells connected to i. We introduce the function $|.|$ that returns the number of elements in a set. The cells i entering the network verify $|\mathcal{P}_i| = 0$, and the ones exiting the network verify $|\mathcal{N}_i| = 0$.

Based on all the network connections $\{\mathcal{P}_i,\ \mathcal{N}_i \mid i \in \mathcal{R}\}$, we define $\mathcal{C}$ as the set of intersections. An intersection connects cells that verify $\mathcal{P}_i \geq 2$ or $\mathcal{N}_i \geq 2$. To each intersection $c \in \mathcal{C}$ is associated the set of its upstream cells $\mathcal{P}_c$ and its downstream cells $\mathcal{N}_c$.

The drivers' behavior at intersections is modeled by split ratios $\beta \in [0, 1]$. For an intersection $c \in \mathcal{C}$, the split ratios represent the fraction of vehicles coming from the upstream

cells $i \in \mathcal{P}_c$ that want to go in each of the downstream cells $i \in \mathcal{N}_c$. We assume that they are known and constant over time. They are subject to

$$\forall c \in \mathcal{C}, \sum_{i \in \mathcal{N}_c} \beta_i = 1 \tag{4}$$

In this study, we consider that all intersections are regulated by TLS. Hence, each intersection $c \in \mathcal{C}$ has $|\mathcal{P}_c|$ cells regulated by a TLS. In the whole network, the number of cells regulated by a TLS is $\sum_{c \in \mathcal{C}} |\mathcal{P}_c|$. The behavior of each TLS is defined on the whole simulation duration T by a function of time $\alpha_i(k)$ that returns 1 (green) or 0 (red), i.e.

$$\forall c \in \mathcal{C}, \forall i \in \mathcal{P}_c, \alpha_i : [0..T] \to \{0, 1\} \tag{5}$$

The functions α_i are fully determined in advance, they must ensure the right of way by verifying at each time step

$$\forall c \in \mathcal{C}, \sum_{i \in \mathcal{P}_c} \alpha_i(k) = 1 \tag{6}$$

Note that α_i are defined as binary functions to reflect the phenomenon of stop-and-go at intersections. This is of particular interest as it has a significant impact on emissions and energy consumption, due to higher accelerations.

2) Cell transmission model: Based on this network characterization, road traffic is modeled at the network level using the CTM. We define dynamic vectors $\rho_k = [\rho_i(k)]_{i \in \mathcal{R}}$ and $u_k = [u_i(k)]_{i \in \mathcal{R}}$ containing respectively the vehicle densities (state) and the speed limits (control) of all cells. The flows of vehicles through the network can be determined from the demands D_i and supplies S_i, defined as

$$D_i(k) = \min\{u_i(k)\rho_i(k) + d_i(k), \varphi^{\mathrm{M}}(u_i(k))\} \tag{7a}$$

$$S_i(k) = \min\{\varphi^{\mathrm{M}}(u_i(k)), \max\{0, w(\rho^{\mathrm{M}} - \rho_i(k))\}\} \tag{7b}$$

where φ^{M} and ρ^{M} denote respectively the maximum flow, that depends on the speed limit u_i, and the maximum density. Each cell i is associated with an endogenous traffic demand term $d_i(k)$, which is a modification of the standard CTM that aims to model the generation of vehicles within the network (vehicles leaving homes, parking lots, etc.).

Moreover, the cells entering and exiting the network are respectively vehicle sources and sinks. Hence, the following parameters are introduced at the network boundaries:

- $d^{\mathrm{in}}(k)$ is the demand on all network entering cells (exogenous traffic demand) at time k, i.e. the vehicles from outside the network that aim at entering it;
- $s^{\mathrm{out}}(k)$ is the network downstream supply, i.e. the vehicles that can leave the network exiting cells at time k.

3) Calibration of the fundamental diagram: The fundamental diagram needs to be calibrated to approximate the behavior of the road users modeled in SUMO. This hypothesis is only valid at steady state. In order to reach such conditions, simulations are run on a ring road, at different density levels. The results are given in Fig. 2, and the associated calibration is presented in Table II. As in [36], the trapezoidal fundamental diagram is considered because it is easy to calibrate, and it is able to capture the bell shape described by the scatter points.

(a) $u = 50\,\mathrm{km/h}$.

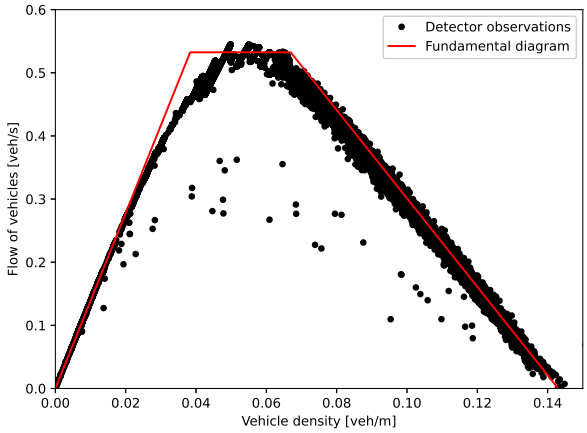

(b) $u = 20\,\mathrm{km/h}$.

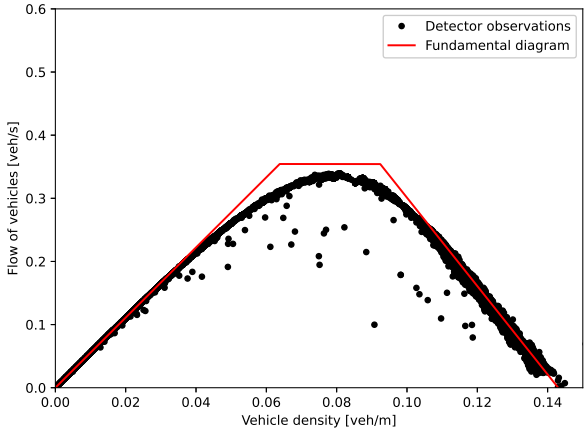

Fig. 2: Fundamental diagrams from ring road simulations, with 50 km/h and 20 km/h speed limits.

It is essential to note that even after the fundamental diagram calibration, the relationship between vehicle density ρ and traffic flow φ remains an approximation insofar as it is true only at steady state.

Symbol	Description	Value	Unit
u	Speed limit (control variable)	u	m/s
w	Backward wave speed	7	m/s
ρ^{M}	Maximum vehicle density	0.143	veh/m
$\varphi^{\mathrm{M}}(u)$	Capacity	$0.8 \times \frac{uw\rho^{\mathrm{M}}}{u+w}$	veh/s

TABLE II: Macroscopic CTM calibrated parameters.

Based on these results, the impact of two different speed limits on the shape of the fundamental diagram is illustrated in Fig. 3.

4) System dynamics: The vehicle flow exiting cell i at time k, denoted $\varphi_i^{\mathrm{out}}(k)$, depends on the number of downstream cells connected to i. It is calculated as indicated in Table III.

Similarly, the vehicle flow entering cell i at time k, denoted $\varphi_i^{\mathrm{in}}(k)$, depends on the number of upstream cells connected to i. It is calculated as indicated in Table IV.

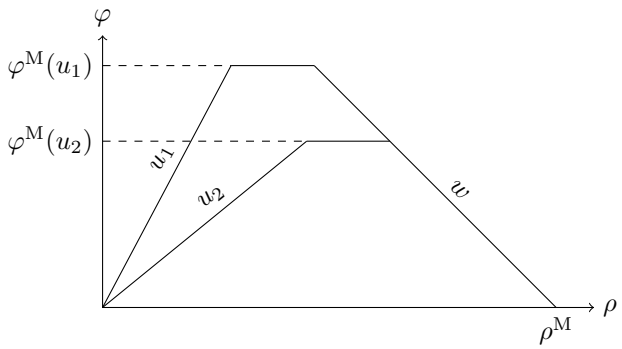

Fig. 3: Fundamental diagrams associated with speed limits u_1 and u_2, where $u_1 > u_2$.

$\lvert\mathcal{N}_i\rvert$	$\varphi_i^{\mathrm{out}}(k)$
0	$\min\left\{D_i(k), \varphi^{\mathrm{M}}(u_i(k)), s^{\mathrm{out}}(k)\right\}$
1	$\min\left\{D_i(k), \varphi^{\mathrm{M}}(u_i(k)), S_{\mathcal{N}_i}(k)\right\}$
≥ 2	$\alpha_i(k)\min\left\{D_i(k), \varphi^{\mathrm{M}}(u_i(k)), \left\{\frac{S_j(k)}{\beta_j}\right\}_{j\in\mathcal{N}_i}\right\}$

TABLE III: Outflows of cells in a network.

Finally, the dynamics of the system is defined as follows

$$\rho_i(k+1) = \rho_i(k) + \frac{\delta_t}{\delta_x}(\varphi_i^{\mathrm{in}}(k) - \varphi_i^{\mathrm{out}}(k)) \tag{8}$$

Based on the fundamental diagram hypothesis and considering that $\varphi = \rho v$, the average traffic speed $v_i(k)$ in cell i at time k can be expressed as

$$v_i(k) = \min\left\{u_i(k), \frac{\varphi^{\mathrm{M}}(u_i(k))}{\rho_i(k)}, w\frac{\rho^{\mathrm{M}} - \rho_i(k)}{\rho_i(k)}\right\} \tag{9}$$

It is essential to keep in mind that this approach determines the average speed for a given density at steady state only. The reason is that the density does not fully characterize the microscopic behavior of vehicles.

III. Energy consumption and pollutant emission models

This section presents the microscopic fuel consumption and NOx emission model, as well as the macroscopic one based on an ANN for prediction purposes.

A. Microscopic fuel consumption and NOx emission model

To calculate the energy consumption and pollutant emissions of vehicles from their trajectories, several microscopic models based on data-driven approaches such as look-up tables [37], regression models [38], and ANN [39] can be found in the literature. Another approach consists in developing a physical microscopic model based on the vehicle's parameters. Such models can be deterministic [40] or stochastic [41]. Their main advantage is their adaptability to any vehicle under any operating conditions.

$\lvert\mathcal{P}_i\rvert$	$\varphi_i^{\mathrm{in}}(k)$
0	$\min\left\{d^{\mathrm{in}}(k), \varphi^{\mathrm{M}}(u_i(k)), S_i(k)\right\}$
1	$\varphi_{\mathcal{P}_i}^{\mathrm{out}}(k)$
≥ 2	$\beta_i \sum_{j\in\mathcal{P}_i} \varphi_j^{\mathrm{out}}(k)$

TABLE IV: Inflows of cells in a network.

In this work, a microscopic physical model is proposed to calculate the energy consumption and NOx emissions of internal combustion engine vehicles one by one, based on their longitudinal dynamics. The list of necessary parameters and variables is given in Table V. They correspond to a Euro 4 diesel passenger car, which represented around 27.8% of the French statistical vehicle fleet in 2017 [42].

Symbol	Description	Value	Unit
C_{rr}	Rolling resistance coefficient	0.007	–
C_{X}	Drag coefficient	0.27	–
F_{a}	Aerodynamic drag	–	N
F_{r}	Rolling resistance force	–	N
F_{w}	Wheel force	–	N
M	Vehicle mass	1340	kg
M_{i}	Vehicle inertial mass	–	kg
R	Wheel radius	0.32	m
R_{BGR}	Burned gas rate	–	%
S	Vehicle cross-section	1.95	m^2
T_{e}	Engine torque	–	N.m
T_{w}	Wheel torque	–	N.m
a_f	Acceleration of vehicle f	–	$\mathrm{m.s}^{-2}$
g	Gravitational acceleration	9.81	$\mathrm{m.s}^{-2}$
m_{fuel}	In-cylinder fuel mass per stroke and displaced volume	–	$\mathrm{g.L}^{-1}\mathrm{.str}^{-1}$
v_f	Speed of vehicle f	–	$\mathrm{m.s}^{-1}$
y^{fuel}	Fuel consumption rate	–	$\mathrm{L.s}^{-1}$
y^{NOx}	NOx emission rate	–	$\mathrm{kg.s}^{-1}$
γ	Gear ratio	–	–
η_{gb}	Gear box efficiency	0.95	–
ρ^{air}	Air density	1.22	$\mathrm{kg.m}^{-3}$
ρ^{fuel}	Fuel density	0.845	$\mathrm{kg.L}^{-1}$
ω_{e}	Engine speed	–	$\mathrm{rad.s}^{-1}$
$\omega_{\max}$	Maximum engine speed	$\frac{4250\times 2\pi}{60}$	$\mathrm{rad.s}^{-1}$
$\omega_{\min}$	Minimum engine speed	$\frac{800\times 2\pi}{60}$	$\mathrm{rad.s}^{-1}$

TABLE V: Microscopic fuel consumption and NOx emission model parameters and variables.

Even in the presence of lateral maneuvers such as lane changes, considering the longitudinal motion alone is sufficient because the energy associated with transient maneuvers can usually be neglected [40]. Under this hypothesis, Newton's second law of motion for a vehicle f at time step k is written

$$(M + M_{\mathrm{i}}(\gamma(k)))a_f(k) = F_{\mathrm{w}}(k) - F_{\mathrm{a}}(k) - F_{\mathrm{r}}(k) \tag{10}$$

where the resistive forces F_{a} and F_{r} represent respectively the aerodynamic drag and the rolling resistance force, and F_{w} denotes the wheel force. They are illustrated in Fig. 4. The vehicle inertial mass M_{i} is defined as a function of the gear ratio $\gamma(k)$, which is updated according to a gear law based on the value of the engine speed. The vehicle acceleration a_f is calculated as the discrete derivative of its speed v_f.

The resistive forces can be calculated as follows

$$F_{\mathrm{a}}(k) = \frac{1}{2}\rho^{\mathrm{air}} S C_{\mathrm{X}} v_f(k)^2 \tag{11a}$$

$$F_{\mathrm{r}}(k) = C_{\mathrm{rr}} M g \tag{11b}$$

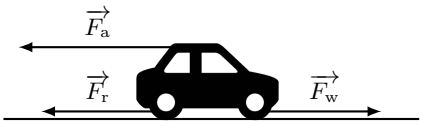

Fig. 4: Forces applied to a moving vehicle.

The wheel force F_{w} is calculated from Eq. 10–11. It can be positive (driver accelerating) or negative (driver braking). The wheel torque is expressed as follows

$$T_{\mathrm{w}}(k) = F_{\mathrm{w}}(k)R \tag{12}$$

The engine torque T_{e} and the engine speed ω_{e} can be directly calculated using the following relationships

$$T_{\mathrm{e}}(k) = \frac{T_{\mathrm{w}}(k)}{\gamma(k)\eta_{\mathrm{gb}}} \tag{13a}$$

$$\omega_{\mathrm{e}}(k) = \min\left\{\max\left\{\frac{v_f(k)\gamma(k)}{R}, \omega_{\min}\right\}, \omega_{\max}\right\} \tag{13b}$$

Based on the engine torque and speed, the fuel consumption rate y^{fuel}, expressed in liters per second, can be given by fuel consumption maps.

The NOx emission rate y^{NOx}, expressed in kilograms per second, is calculated from y^{fuel}, the burned gas rate R_{BGR}, and the in-cylinder fuel mass per stroke and displaced volume m_{fuel} [43]. It reads

$$\log\left(\frac{y^{\mathrm{NOx}}}{y^{\mathrm{fuel}}\rho^{\mathrm{fuel}}}\right) = a_1 + a_2 R_{\mathrm{BGR}} + a_3 m_{\mathrm{fuel}} \tag{14}$$

where a_1 – a_3 are regression coefficients. Finally, the total fuel consumption and NOx emissions in the whole network between time steps 0 and T can be calculated as follows

$$E^{0\to T} = \sum_{k=0}^{T}\sum_{p}\delta_t y_p^{\mathrm{fuel}}(k) \tag{15a}$$

$$NOx^{0\to T} = \sum_{k=0}^{T}\sum_{p}\delta_t y_p^{\mathrm{NOx}}(k) \tag{15b}$$

B. Macroscopic fuel consumption model

To control the traffic system in an energy efficient way, it is essential to calibrate a macroscopic energy model that predicts the fuel consumption from the CTM variables. This point is challenging as such data do not contain all the information on individual vehicles' behavior. Hence, the macroscopic energy model associates the same fuel consumption rate to all the vehicles of the same cell at a given time.

As detailed in [33], we propose to calibrate an ANN, using SUMO simulation data generated with the road network given in Fig. 7. The training data are measured at a sampling frequency of 1 Hz, generating about 3.5 million data points.

The ANN predicts the average fuel consumption rate per vehicle in cell i at time k, expressed in liters per second per vehicle and denoted $\hat{y}_i^{\mathrm{fuel}}(k)$. It is composed of three hidden layers (of 24, 16, and 8 nodes). All nodes of each layer use the rectifier activation function that returns the positive part of its argument. The ANN has the following inputs.

$$\hat{y}_i^{\mathrm{fuel}}(k) = f(\rho_i(k), \rho_i(k-1), v_i(k), v_i(k-1), u_i(k), \alpha_i(k)) \tag{16}$$

In case cell i is not regulated by a TLS, we consider $\forall k, \alpha_i(k) = 1$. The densities and speeds at previous time steps are included in the model inputs as they add information on the dynamics of the system. This partially compensates for the fact that the macroscopic CTM variables do not contain any information on vehicles accelerations.

As a result, for predicted densities $\hat{\rho}^{\tau+1\to\tau+\Delta_p}$ in the whole network over a prediction time horizon Δ_p (between time steps $\tau+1$ and $\tau+\Delta_p$), the associated predicted total fuel consumption, expressed in liters, is

$$\hat{E}^{\tau+1\to\tau+\Delta_p} = \sum_{k=\tau+1}^{\tau+\Delta_p}\sum_{i\in\mathcal{R}}\delta_x\delta_t\hat{\rho}_i(k)\hat{y}_i^{\mathrm{fuel}}(k) \tag{17}$$

IV. Eco-VSL controller

In this section, we present the eco-VSL controller aiming at improving traffic energy efficiency. The approach is based on a closed-loop NMPC control framework summarized in Fig. 5.

In the literature, NMPC strategies constitute a commonly used methodology to control traffic systems [17]. Yet, [44] highlights some shortcomings due to models inaccuracy, the unpredictable gaming activity associated with route choices, and the chaotic behavior of road networks under heavy congestion. To alleviate these issues, this work is positioned downstream of the traffic assignment problem: the origin-destination matrices and routes are fully determined in advance. They are randomly generated by the traffic simulator to be compliant with the split ratios, which are not controlled. In practice, the controller operates as follows:

1) At each control time step τ, i.e. multiple of the control time horizon Δ_c, the current state of the system ρ_τ is measured and provided to the NMPC controller.
2) The traffic predictor estimates the evolution of the system state $\hat{\rho}^{\tau+1\to\tau+\Delta_p}$ on a prediction time horizon Δ_p, i.e. between $\tau+1$ and $\tau+\Delta_p$
3) The ANN-based macroscopic fuel consumption model is used to predict the energy consumption $\hat{E}^{\tau+1\to\tau+\Delta_p}$ on the same horizon Δ_p.
4) An optimizer based on the Broyden-Fletcher-Goldfarb-Shanno (BFGS) algorithm repeats steps 2 and 3 to find system inputs, i.e. a trajectory of speed limits $u^{\tau+1\to\tau+\Delta_p}$, that minimizes an objective function J along horizon Δ_p. Once the optimum is found, its first iteration (between $\tau+1$ and $\tau+\Delta_c$) is applied.
5) Finally, the performance of the controller is evaluated by calculating the energy consumption $E^{0\to T}$ and NOx emission levels $NOx^{0\to T}$ a posteriori of the simulation from the vehicles' individual speed profiles, using the microscopic physical model.

The BFGS algorithm is an iterative method able to solve unconstrained nonlinear optimization problems. It is based on an approximation of the inverse of the second derivative of the objective function, rather than explicitly constructing the

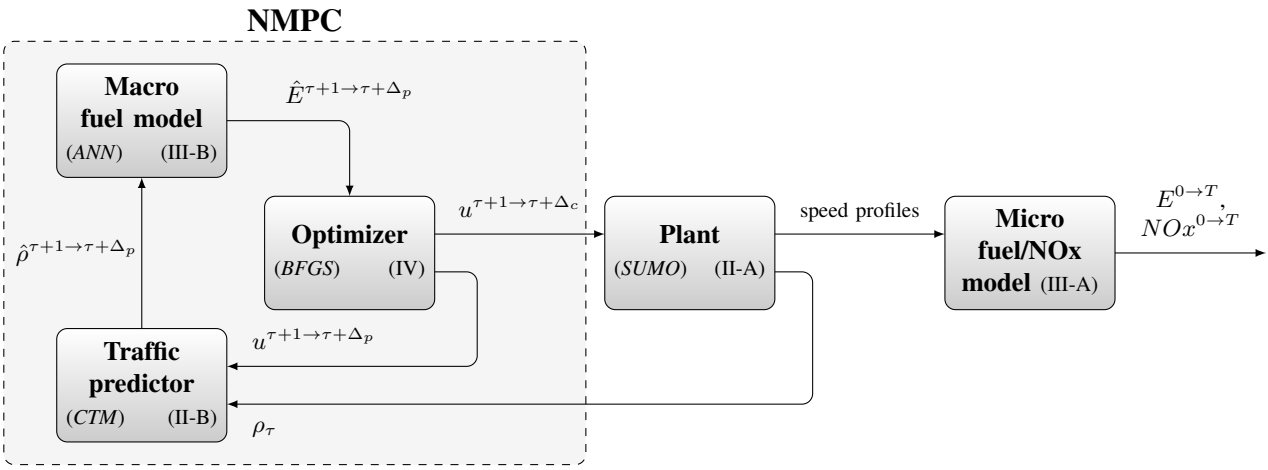

Fig. 5: Block diagram of the global approach for ecological variable speed limits.

Hessian matrix. In practice, this approximation is obtained from gradient evaluations via a secant method. As a result, the computational complexity of the algorithm is only $\mathcal{O}(n^2)$. This quasi-Newton method has global convergence properties on uniformly convex problems [45], which is not the case in this work. The limited-memory version L-BFGS-B [46] is used here. It is particularly suited to high-dimensional problems and handles bound constraint minimization, which is necessary to remain within the allowable speed limits.

To improve the performance of the solver, L-BFGS-B is used in a two-phase method that combines a global stepping algorithm with local minimization. In total, we consider in this work 6 runs of the local minimizer to improve the global solution and to reduce the risk of local optimum. As a result, the controller takes an average of 8 min 30 s to run at each control time step, which makes it compatible with off-line approaches only.

For implementation reasons, the prediction time horizon Δ_p should be a multiple of the control time horizon Δ_c. The corresponding proportionality coefficient κ is defined as

$$\exists \kappa \in \mathbb{N}^*,\ \Delta_p = \kappa \Delta_c \tag{18}$$

The operation of the NMPC controller is illustrated in Fig. 6. To simplify its implementation, it is parameterized as follows:

- Between two successive control time steps τ and $\tau + \Delta_c$, the control (speed limits) remain constant. It is continuous and bounded by $20\,\mathrm{km/h}$ and $50\,\mathrm{km/h}$.
- All the cells of a given road have the same speed limit.
- To reduce the degree of freedom of the system, the trajectory of speed limits are parameterized by grouping the roads in a few clusters. Each cluster is then controlled by a single control variable, i.e. all the roads of the same cluster are subject to the same speed limit at any time of the simulation. A counterpart of this approach is that the solution obtained may be suboptimal. However, it is usually necessary when going large scale because considering n_{MPC} clusters of roads results in an optimization problem with $\kappa \times n_{\mathrm{MPC}}$ variables only at each control time step. In practice, κ and n_{MPC} can both be adapted to have convenient computation times. The choice of the value of κ should be a compromise between the computational burden and the robustness of the controller. The choice of n_{MPC} mainly depends on the structure of the network.

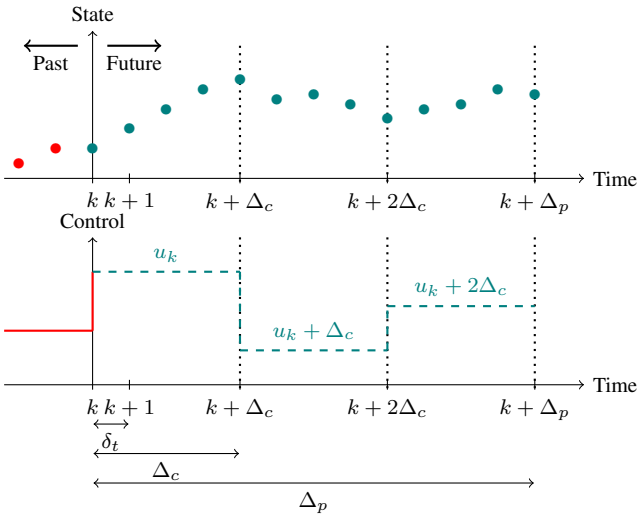

Fig. 6: Representation of the NMPC framework, for $\kappa = 3$.

The choice of the objective function is crucial in traffic eco-management control strategies. Several formulations can be implemented [3]. Usually, the weighted sum of an ecological metric, and a traffic efficiency metric is considered. The purpose of this multi-objective optimization, based on metrics that can be antagonistic, is to avoid trivial solutions (for example, reduce the speed limits of the entering roads to reduce the number of vehicles in the network, which will naturally reduce the fuel consumption), and find a compromise between energy efficiency and traffic performance. In this study, we propose to define the objective function as the ratio between the predicted total fuel consumption $\hat{E}^{\tau+1\to\tau+\Delta_p}$ and the predicted total travel distance $\hat{TTD}^{\tau+1\to\tau+\Delta_p}$ between $\tau+1$ and $\tau+\Delta_p$. Minimizing this ratio is relevant for optimizing the traffic energy efficiency as it corresponds to the average fuel consumption of a vehicle per unit distance. Usually, it is

expressed in liters per 100 kilometers traveled. The predicted total travel distance $\hat{TTD}^{\tau+1\to\tau+\Delta_p}$ is expressed in meters and can be calculated as follows

$$\hat{TTD}^{\tau+1\to\tau+\Delta_p} = \sum_{k=\tau+1}^{\tau+\Delta_p} \sum_{i\in\mathcal{R}} \delta_x \delta_t \hat{\rho}_i(k) \hat{v}_i(k) \tag{19}$$

The resulting objective function J is given below. Note that the use of the total travel distance in the objective might seem counter-intuitive at first glance as route choices are defined before the simulation, and are not affected by the controller. However, its value on the prediction horizon, which is a given and limited time interval, is affected by the traffic conditions.

$$J = \frac{\hat{E}^{\tau+1\to\tau+\Delta_p}}{\hat{TTD}^{\tau+1\to\tau+\Delta_p}} = \frac{\sum_{k=\tau+1}^{\tau+\Delta_p} \sum_{i\in\mathcal{R}} \hat{\rho}_i(k) \hat{y}_i^{\text{fuel}}(k)}{\sum_{k=\tau+1}^{\tau+\Delta_p} \sum_{i\in\mathcal{R}} \hat{\rho}_i(k) \hat{v}_i(k)} \tag{20}$$

V. Simulations and Results

This section evaluates the performance of the eco-VSL controller. The results are analyzed both in terms of environmental sustainability and traffic performance.

A. Case study

We propose to consider the road network represented in Fig. 7. It is composed of an urban (38 roads of 300 meters represented by solid lines) and a peri-urban (7 roads of 2400 meters represented by dashed lines) area. In this study, the VSL strategy is implemented in the urban area only. The peri-urban area, whose roads can be seen as highway links leading to the urban area, have a constant speed limit of 70 km/h. The consideration of the peri-urban area in this study is crucial in order to get a complete picture and evaluate the impact of the controller on environmental sustainability and traffic performance at the boundary roads, if queues are appearing for example.

In the CTM, all the roads have the same spatial discretization with cells of 60 m, i.e. 5 cells in the urban roads and 40 cells in the peri-urban roads. At each intersection, both downstream roads have a split ratio of 0.5 and all TLS have cycles of 88 s (44 s green and 44 s red). Also, all TLS are synchronized in the sense that the offsets are zero for all intersections. In the context of this study, the consideration of lane changes is not really significant in the analysis of pollutant emissions and fuel consumption. We therefore propose to limit this problem to the longitudinal dynamics of vehicles only by considering one-lane roads.

In order to evaluate the controller performance and analyze its operating range, three time-varying traffic demand scenarios are proposed in Fig. 8. They are parameterized as follows:

- As represented in Fig. 7, exogenous (black dots) and endogenous (red dots) vehicle sources are considered. The reason is that it is difficult to significantly increase the level of congestion in this kind of network simply by varying the generation rate at the border exogenous sources. This is mainly due to the presence of TLS at each intersection, and to the fact that all roads have the same capacity. Scenario (a) is conducive to the study of transition phases between different traffic states, Scenario (b) corresponds to a network unlikely to decongest because of a constant endogenous traffic demand, and Scenario (c) depicts a free-flow situation.
- The simulation duration is $T = 1\,\text{h}$. The control time horizon Δ_c is set at 1 min and the prediction time horizon Δ_p is set at 5 min, i.e. $\kappa = 5$. Note that Δ_c is set longer than the simulation time step $\delta_t = 1\,\text{s}$ in order to make the controller more realistic.
- In order to reduce the computational burden, two clusters of roads are defined and identified in Fig. 7. Each cluster is controlled with the same variable. Due to the simple network architecture, the first one is composed of the roads at the interface between the urban and the peri-urban area. The other one is composed of the inner urban roads. The peri-urban area is not controlled but the effect of the control of the urban area on the peri-urban area is investigated in detail.

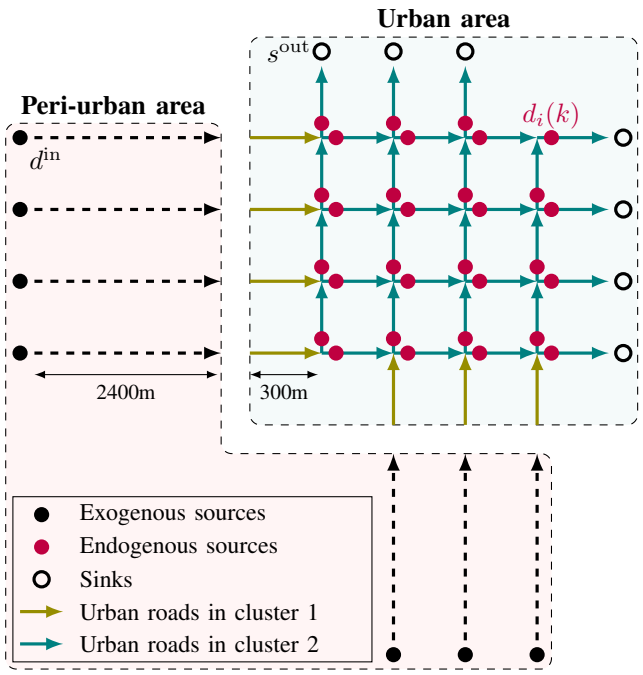

Fig. 7: Road network composed of urban (solid lines) and peri-urban (dashed lines) areas. Urban roads of the same color are in the same cluster and hence have the same speed limit.

The number and size of clusters defined above are critical points. In the scenarios under study, the proposed clusters are particularly suitable because of the network architecture. The definition of the clusters is more complex in more realistic road networks because they must integrate the dynamics of congestion. A compromise needs to be found between the controller performance on the one hand and its computational burden, higher risk to reach local minima, and too much variability in the speed limit from one street to another on the other hand.

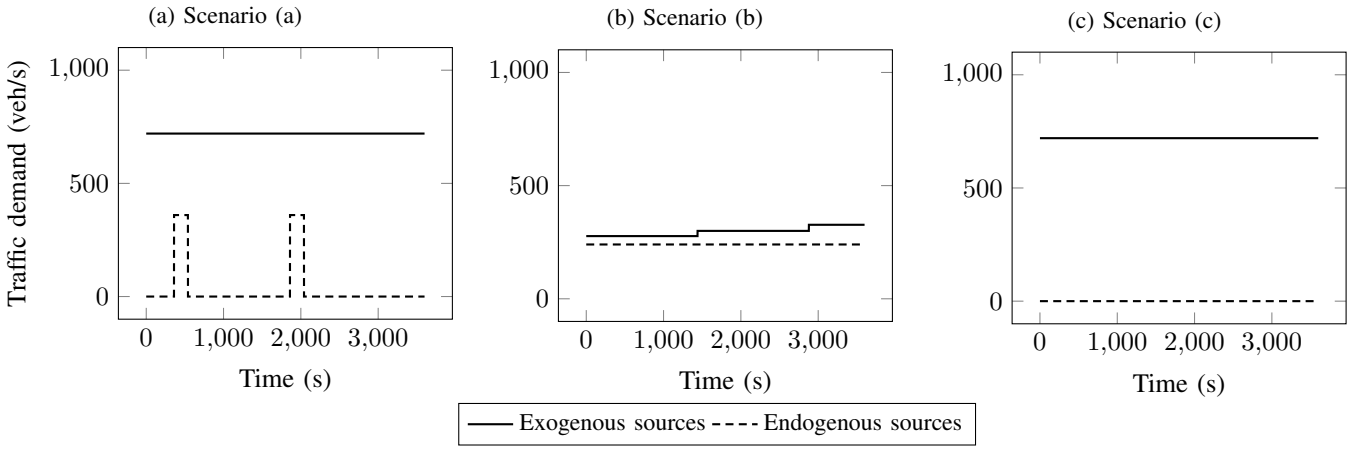

Fig. 8: Traffic demand scenarios at exogenous and endogenous vehicle sources.

B. Results of eco-VSL approach

For each traffic demand scenario, the energy efficiency, NOx emission levels, and traffic performance of the closed-loop eco-VSL approach are compared with two baseline simulations that have constant speed limits:

- *Open-loop 30 km/h*: speed limits of 30 km/h in urban and 70 km/h in peri-urban area.
- *Open-loop 50 km/h*: speed limits of 50 km/h in urban and 70 km/h in peri-urban area.

The optimal dynamic speed limits found by the eco-VSL controller in each scenario are given in Fig. 9. The figures also provide the evolution of the number of vehicles in the urban area. Scenario (a) reveals that in situations of peak demand, the controller is able to decongest the network faster than the baseline scenarios, thus limiting the number of vehicles simultaneously present in the controlled area.

For each scenario, the metrics measured with eco-VSL and in the open-loop 30 km/h and 50 km/h simulations are gathered in Table VI. Both ecological (average fuel consumption and NOx emissions) and traffic performance (TTD and number of arrived vehicles) metrics are analyzed. They are always measured both in the urban and the peri-urban areas. In the urban area, the number of arrived vehicles corresponds to those that went in one of the sinks, and in the peri-urban area, it corresponds to those that have entered the urban area.

The results of scenario (a) indicate that the controller is able to reduce the average fuel consumption in the urban area, which corresponds to the objective function, from 7.7 L/100km to 6.5 L/100km, i.e. by approximately 16%. On a macroscopic scale, the total fuel consumption (in both areas) during 1 h is 1167 L in the open-loop 30 km/h approach and 998 L in the closed-loop control approach. This gap corresponds to a total reduction of 451 kilograms of CO2. Thanks to a faster decongestion of the urban area, the lengths of queues in the peri-urban roads are reduced. This results in a reduction of the average fuel consumption on these roads also (respectively 29% and 5% reduction with the 30 km/h and 50 km/h baseline scenarios).

Similarly, the faster decongestion performed by the controller results in a reduction of NOx emissions in both areas. In comparison with the open-loop 30 km/h approach, the controller reduced the average NOx emissions by 14% in the urban area and by 27% in the peri-urban area. In comparison with the open-loop 50 km/h approach, the controller reduced the average NOx emissions by 16% in the urban area and by 7% in the peri-urban area.

In addition to the average fuel consumption and NOx emissions reduction, the controller also improves traffic fluidity. In comparison with the open-loop 30 km/h approach, the controller increases the TTD by 16% in the urban area and by 4% in the peri-urban area. In comparison with the open-loop 50 km/h approach, the controller increases the TTD by 4% in the urban area and by 1% in the peri-urban area. This indicates that, despite a lower number of vehicles present in the urban area at each moment of the simulation (cf. Fig. 9a), eco-VSL improves the global flow of vehicles.

The improvement of traffic fluidity is also highlighted by the number of arrived vehicles. In total, 940 and 259 more vehicles have completed their journeys, i.e. have reached a sink, in the closed-loop control scenario, in comparison with the open-loop 30 km/h and 50 km/h approaches respectively.

It is interesting to note that inside the urban area, the controller keeps a speed limit close to 50 km/h. This can be interpreted as a way to accelerate the decongestion of the network, as 50 km/h speed limits constitute a good compromise between average fuel consumption and TTD.

Note that the controller could be more realistic by limiting the possible speed limits to multiple of 5 km/h, for example. A simulation has been made by rounding the controller outputs in this way. The resulting average fuel consumption is 6.8 L/100km, i.e. a reduction of 12% (instead of 16% with continuous speed limits values) in comparison with the baseline scenarios.

Scenarios (b) and (c) can be seen as borderline cases. In fact, scenario (b) is unlikely to decongest, even with the eco-VSL, because of the continuous endogenous demand. Scenario (c) results in a free-flow situation because of the absence of endogenous traffic demand. As a result, it appears that a 50 km/h speed limit is optimal in both situations because it is the best compromise between energy efficiency and traffic

Scenario	Simulation	Fuel Consumption (L/100km)		NOx emissions (mg/km)		Total travel distance (km)		Arrived vehicles (veh)	
		Urban	Peri-urban	Urban	Peri-urban	Urban	Peri-urban	Urban	Peri-urban
(a)	30 km/h	7.7	5.5	3329	2516	6907	11514	5306	4446
	50 km/h	7.7	4.2	3388	1978	7741	11889	5987	4957
	eco-VSL	6.5	3.9	2862	1848	8026	12001	6246	5077
(b)	30 km/h	17.9	10.0	7841	4464	3882	4291	4675	1031
	50 km/h	15.0	8.6	6657	3883	4938	4479	5619	1185
	eco-VSL	14.8	8.4	6598	3812	4830	4515	5594	1206
(c)	30 km/h	5.4	3.3	2289	1576	7193	12085	5162	5195
	50 km/h	4.9	3.2	2148	1552	7308	12043	5290	5195
	eco-VSL	5.0	3.3	2214	1569	7297	12054	5290	5195

TABLE VI: Comparison of the ecological and the traffic performance metrics measured when the online ecological VSL approach is performed, with baseline scenarios that have constant speed limits of 30 km/h and 50 km/h.

performance in these steady states. In this sense, Fig. 9 shows that the control tends towards this value in both scenario, resulting in very similar results regarding the energy efficiency and the traffic performance. For example, differences of less than 2% with the baseline 50 km/h speed limits simulation are observed for the average fuel consumption.

In brief, the developed closed-loop control strategy is particularly efficient in situations of transition between different congestion levels. In fact, it appears that the controller is able to decongest the network much faster than in the open-loop simulations. This results in an improvement of both the ecological and the traffic performance metrics. Most importantly, these metrics are not only improved inside the controlled network, but also at its boundaries, i.e. in the uncontrolled peri-urban area. However, it appears that with the very basic road network considered, the controller is not able to significantly improve the metrics in fully congested or completely free-flow situations. These borderline scenarios can be qualified as non-controllable. In these cases, the best results seem to be obtained with constant 50 km/h speed limits.

VI. Discussion and conclusions

In this work, the impact of ecological VSLs on environmental sustainability and traffic performance in a synthetic urban network is analyzed.

This study introduces microscopic traffic, energy consumption, and NOx emission models. In order to implement a closed-loop eco-VSL strategy, a macroscopic traffic model and a macroscopic fuel consumption model, which is based on an ANN, are calibrated in order to predict and minimize the average fuel consumption per vehicle and per distance traveled.

The results indicate that the proposed eco-VSL controller has a great potential to maintain the system at desired density levels, and ensures smoother transitions between different levels of congestion. This results in a significant reduction in fuel consumption and emissions, as well as a smoother and more efficient road traffic. The closed-loop control strategy is able to improve the environmental sustainability and traffic performance in the controlled urban area and at the network boundaries, i.e. in the uncontrolled peri-urban area. The analysis of additional scenarios shows that the eco-VSL controller is mostly effective during transient phases, such as demand peaks that lead to congestion.

In this work, a synthetic artificial network is simulated in SUMO traffic simulator, with the IDM. The proposed approach can be easily adapted to more realistic and asymmetric networks that lead to more complex traffic dynamics. In fact, several roads of different length, capacity, and traffic demand are supposed to increase the potential of this closed-loop control approach. In practice, this would be associated with the identification of road clusters to determine areas of interest and an appropriate tuning of the parameters of the controller (more clusters with less roads in each cluster to improve the performance, etc.) and the macroscopic traffic model (different fundamental diagrams associated with roads of different number of lanes, etc.).

One main challenge of implementing this kind of control schemes in a real-world setting lies in the communication of speed limits at all times to all vehicles. This suggests the use of connectivity for an optimal control. This approach is also subject to the respect of speed limits by road users.

Finally, the fact that the proposed controller seems mostly effective in transient phases between different congestion situations motivates the exploration of control strategies that combine eco-VSL with vehicle-based approaches. These include for example eco-driving, eco-routing, and cooperation strategies.

References

[1] K. Balakrishnan, S. Dey, T. Gupta, R. Dhaliwal, M. Brauer, A. J. Cohen, J. D. Stanaway, G. Beig, T. K. Joshi, A. N. Aggarwal, et al., "The impact of air pollution on deaths, disease burden, and life expectancy across the states of india: the global burden of disease study 2017," The Lancet Planetary Health, vol. 3, no. 1, pp. e26–e39, 2019.

[2] J. M. Samet, F. Dominici, F. C. Curriero, I. Coursac, and S. L. Zeger, "Fine particulate air pollution and mortality in 20 us cities, 1987–1994," New England journal of medicine, vol. 343, no. 24, pp. 1742–1749, 2000.

[3] B. Othman, G. De Nunzio, D. Di Domenico, and C. Canudas-de-Wit, "Ecological traffic management: A review of the modeling and control strategies for improving environmental sustainability of road transportation," Annual Reviews in Control, vol. 48, pp. 292 – 311, 2019.

(a) Scenario (a)

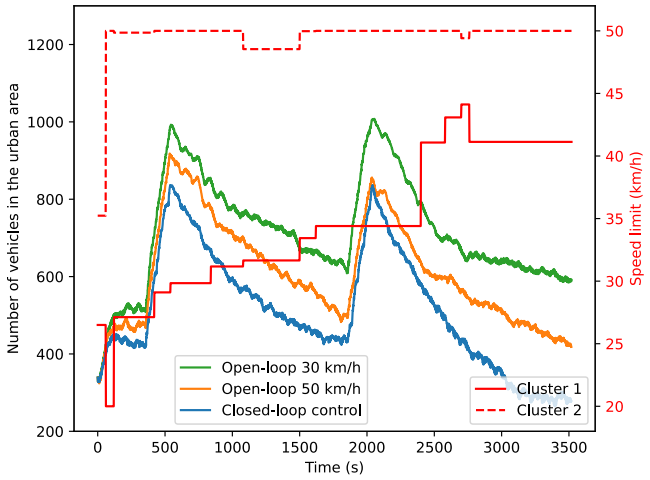

(b) Scenario (b).

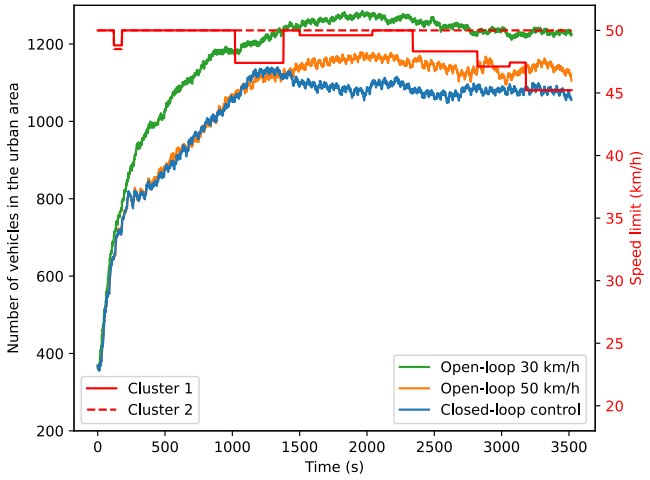

(c) Scenario (c).

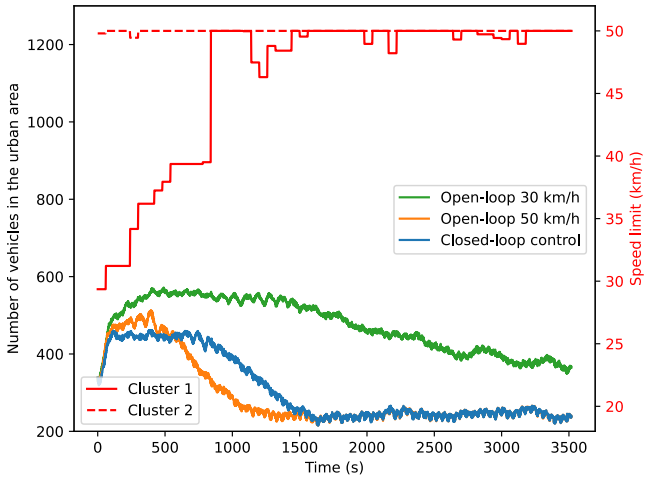

Fig. 9: Evolution of the optimal speed limits in clusters 1 and 2, as well as the number of vehicles in the urban area.

[4] A. Sciarretta and A. Vahidi, Energy Saving Potentials of CAVs, pp. 1–31. Cham: Springer International Publishing, 2020.

[5] J. D. Vreeswijk, M. Mahmod, and B. van Arem, "Energy efficient traffic management and control-the ecomove approach and expected benefits," in 13th International IEEE Conference on Intelligent Transportation Systems, pp. 955–961, IEEE, 2010.

[6] G. De Nunzio, I. B. Gharbia, and A. Sciarretta, "A general constrained optimization framework for the eco-routing problem: Comparison and analysis of solution strategies for hybrid electric vehicles," Transportation Research Part C: Emerging Technologies, vol. 123, p. 102935, 2021.

[7] L. Thibault, G. D. Nunzio, and A. Sciarretta, "A unified approach for electric vehicles range maximization via eco-routing, eco-driving, and energy consumption prediction," IEEE Transactions on Intelligent Vehicles, vol. 3, pp. 463–475, 2018.

[8] Y. Huang, E. C. Ng, J. L. Zhou, N. C. Surawski, E. F. Chan, and G. Hong, "Eco-driving technology for sustainable road transport: A review," Renewable and Sustainable Energy Reviews, vol. 93, pp. 596–609, 2018.

[9] C. Pasquale, I. Papamichail, C. Roncoli, S. Sacone, S. Siri, and M. Papageorgiou, "Two-class freeway traffic regulation to reduce congestion and emissions via nonlinear optimal control," Transportation Research Part C: Emerging Technologies, vol. 55, pp. 85–99, 2015.

[10] A. Csikós, T. Luspay, and I. Varga, "Modeling and optimal control of travel times and traffic emission on freeways," IFAC Proceedings Volumes, vol. 44, no. 1, pp. 13058 – 13063, 2011. 18th IFAC World Congress.

[11] K. Han, H. Liu, V. V. Gayah, T. L. Friesz, and T. Yao, "A robust optimization approach for dynamic traffic signal control with emission considerations," Transportation Research Part C: Emerging Technologies, vol. 70, pp. 3–26, 2016.

[12] C. Osorio and K. Nanduri, "Energy-efficient urban traffic management: a microscopic simulation-based approach," Transportation Science, vol. 49, no. 3, pp. 637–651, 2015.

[13] J. Zhao, W. Li, J. Wang, and X. Ban, "Dynamic traffic signal timing optimization strategy incorporating various vehicle fuel consumption characteristics," IEEE Transactions on Vehicular Technology, vol. 65, no. 6, pp. 3874–3887, 2015.

[14] M. Madireddy, B. De Coensel, A. Can, B. Degraeuwe, B. Beusen, I. De Vlieger, and D. Botteldooren, "Assessment of the impact of speed limit reduction and traffic signal coordination on vehicle emissions using an integrated approach," Transportation research part D: transport and environment, vol. 16, no. 7, pp. 504–508, 2011.

[15] M. Taylor, "Network modeling of the traffic, environmental and energy effects of lower urban speed limits," Road and Transport Research, vol. 9, pp. 48–57, 12 2000.

[16] E. Walraven, M. T. Spaan, and B. Bakker, "Traffic flow optimization: a reinforcement learning approach," Engineering Applications of Artificial Intelligence, vol. 52, pp. 203 – 212, 2016.

[17] M. Tajali and A. Hajbabaie, "Dynamic speed harmonization in urban street networks," Computer-Aided Civil and Infrastructure Engineering, 03 2018.

[18] M. Hadiuzzaman and T. Z. Qiu, "Cell transmission model based variable speed limit control for freeways," Canadian Journal of Civil Engineering, vol. 40, no. 1, pp. 46–56, 2013.

[19] A. Hegyi, S. P. Hoogendoorn, M. Schreuder, H. Stoelhorst, and F. Viti, "Specialist: A dynamic speed limit control algorithm based on shock wave theory," in 2008 11th International IEEE Conference on Intelligent Transportation Systems, pp. 827–832, 2008.

[20] Y. Zu, C. Liu, R. Dai, A. Sharma, and J. Dong, "Real-time energy-efficient traffic control via convex optimization," Transportation Research Part C: Emerging Technologies, vol. 92, pp. 119 – 136, 2018.

[21] S. K. Zegeye, B. De Schutter, J. Hellendoorn, E. A. Breunesse, and A. Hegyi, "A predictive traffic controller for sustainable mobility using parameterized control policies," IEEE Transactions on Intelligent Transportation Systems, vol. 13, no. 3, pp. 1420–1429, 2012.

[22] B. Khondaker and L. Kattan, "Variable speed limit: a microscopic analysis in a connected vehicle environment," Transportation Research Part C: Emerging Technologies, vol. 58, pp. 146 – 159, 2015.

[23] L. Tumash, C. Canudas de Wit, and M. L. Delle Monache, Boundary and VSL Control for Large-Scale Urban Traffic Networks, 2021. Working paper or preprint, available at https://hal.archives-ouvertes.fr/hal-03167733.

[24] M. Van den Berg, A. Hegyi, B. De Schutter, and H. Hellendoorn, "Integrated traffic control for mixed urban and freeway networks: A model predictive control approach," European Journal of Transport and Infrastructure Research EJTIR, 7 (3), 2007.

[25] B. Khondaker and L. Kattan, "Variable speed limit: an overview," Transportation Letters, vol. 7, no. 5, pp. 264–278, 2015.

[26] G. De Nunzio, C. Canudas-de-Wit, and P. Moulin, "Urban traffic eco-driving: A macroscopic steady-state analysis," in Control Conference (ECC), 2014 European, pp. 2581–2587, IEEE, 2014.

[27] B. Othman, G. De Nunzio, D. Di Domenico, and C. Canudas-de-Wit, "Variable speed limits control in an urban road network to reduce environmental impact of traffic," in 2020 Annual American Control Conference (ACC), pp. 1179–1184, IEEE, 2020.

[28] F. Soriguera, I. Martínez, M. Sala, and M. Menéndez, "Effects of low speed limits on freeway traffic flow," Transportation Research Part C: Emerging Technologies, vol. 77, pp. 257–274, 2017.

[29] M. Papageorgiou, E. Kosmatopoulos, and I. Papamichail, "Effects of variable speed limits on motorway traffic flow," Transportation Research Record, vol. 2047, no. 1, pp. 37–48, 2008.

[30] M. Treiber, A. Hennecke, and D. Helbing, "Congested traffic states in empirical observations and microscopic simulations," Physical review E, vol. 62, no. 2, p. 1805, 2000.

[31] M. Pourabdollah, E. Bjärkvik, F. Fürer, B. Lindenberg, and K. Burgdorf, "Calibration and evaluation of car following models using real-world driving data," in 2017 IEEE 20th International Conference on Intelligent Transportation Systems (ITSC), pp. 1–6, IEEE, 2017.

[32] P. A. Lopez, M. Behrisch, L. Bieker-Walz, J. Erdmann, Y.-P. Flötteröd, R. Hilbrich, L. Lücken, J. Rummel, P. Wagner, and E. Wießner, "Microscopic traffic simulation using sumo," in The 21st IEEE International Conference on Intelligent Transportation Systems, IEEE, 2018.

[33] B. Othman, G. De Nunzio, D. Domenico, and C. Canudas-De-Wit, "Urban road traffic fuel consumption optimization via variable speed limits or signalized access control: A comparative study," in IEEE Conference on Decision and Control (CDC) 2021, 2021.

[34] D. Helbing, "Improved fluid-dynamic model for vehicular traffic," Physical Review E, vol. 51, no. 4, p. 3164, 1995.

[35] H. H. Salem, J. Chrisoulakis, M. Papageorgiou, N. Elloumi, and P. Papadakos, "The use of metacor tool for integrated urban and interurban traffic control. evaluation in corridor peripherique, paris," in Proceedings of VNIS'94-1994 Vehicle Navigation and Information Systems Conference, pp. 645–650, IEEE, 1994.

[36] C. F. Daganzo, "The cell transmission model: A dynamic representation of highway traffic consistent with the hydrodynamic theory," Transportation Research Part B: Methodological, vol. 28, no. 4, pp. 269–287, 1994.

[37] K. Post, J. Kent, J. Tomlin, and N. Carruthers, "Fuel consumption and emission modelling by power demand and a comparison with other models," Transportation Research Part A: General, vol. 18, no. 3, pp. 191–213, 1984.

[38] K. Ahn, "Microscopic fuel consumption and emission modeling," Master's thesis, Virginia Tech, 1998.

[39] Z. Xu, Y. Kang, and W. Lv, "Analysis and prediction of vehicle exhaust emission using ann," in 2017 36th Chinese Control Conference (CCC), pp. 4029–4033, IEEE, 2017.

[40] A. Sciarretta and A. Vahidi, Fundamentals of Vehicle Modeling, pp. 33–62. Cham: Springer International Publishing, 2020.

[41] D. Karbowski, N. Kim, and A. Rousseau, "Route-based online energy management of a phev and sensitivity to trip prediction," in Vehicle Power and Propulsion Conference (VPPC), 2014 IEEE, pp. 1–6, IEEE, 2014.

[42] CITEPA, "Gaz à effet de serre et polluants atmosphériques. Bilan des émissions en France de 1990 à 2018," tech. rep., 2020.

[43] L. Thibault, P. Degeilh, O. Lepreux, L. Voise, G. Alix, and G. Corde, "A new gps-based method to estimate real driving emissions," in 2016 IEEE 19th International Conference on Intelligent Transportation Systems (ITSC), pp. 1628–1633, 2016.

[44] C. F. Daganzo, "Urban gridlock: Macroscopic modeling and mitigation approaches," Transportation Research Part B: Methodological, vol. 41, no. 1, pp. 49–62, 2007.

[45] D. C. Liu and J. Nocedal, "On the limited memory bfgs method for large scale optimization," Mathematical programming, vol. 45, no. 1, pp. 503–528, 1989.

[46] C. Zhu, R. H. Byrd, P. Lu, and J. Nocedal, "Algorithm 778: L-bfgs-b: Fortran subroutines for large-scale bound-constrained optimization," ACM Transactions on mathematical software (TOMS), vol. 23, no. 4, pp. 550–560, 1997.

Bassel Othman received the M.Sc degree from the engineering school Ecole des Mines de Saint-Etienne, France, in 2018. He received the Ph.D. in Automatic Control from Grenoble Alpes University, France, in 2021. He is currently a Research Enginner at IFP Energies nouvelles, Lyon, France. His main research interests include modeling and control of transportation and mobility systems, machine learning, optimization, and data analysis and processing.

Giovanni De Nunzio received the B.Sc. and M.Sc. degree in Information and Automation Engineering from the University of L'Aquila, Italy, in 2007 and 2010. He received the Ph.D. in Automatic Control from the Grenoble Institute of Technology (Grenoble INP), France, in 2015. He is currently a Research Engineer and an R&I Project Leader at IFP Energies nouvelles, Lyon, France. His research activities focus on modeling and control of transportation and mobility systems, advanced driver-assistance systems, graph theory, optimization and data science.

Domenico Di Domenico received the M.Sc. degree in Physics from the "Università degli studi di Napoli - Federico II". He received his Ph.D. in Automatic Control from the "Università del Sannio", in 2008. He has been a visiting student at the University of Michigan in Ann Arbor, USA, in 2008. Then, he has been a Postdoctoral Fellow and a Research Engineer at IFP Energies nouvelles in Lyon, France, from 2009 to 2021. He is currently a Research Engineer at TotalEnergies. His research activities are mainly focused on the dynamic modeling and control of electric power sources and energy storage systems.

Carlos Canudas de Wit received his B.Sc. degree in electronics and communications from the Technological Institute of Monterrey, Mexico in 1980. In 1984 he received his M.Sc. in the Department of Automatic Control, Grenoble, France. In 1987 he received his Ph.D. in automatic control from the Polytechnic of Grenoble (Department of Automatic Control), France. Since then he has been working at the same department as Director of Research at the CNRS, where he teaches and conducts research in the area of control systems. He is part of the NeCS GIPSA-Lab team on Networked Controlled Systems and has established several industrial collaboration projects with major French companies. He has been associate editor of the IEEE-Transaction on Automatic Control, from 1992 to 1997, AUTOMATICA, from 1999 to 2002. He is currently Associated Editor of: the Asian Journal of Control (since 2010), IEEE Transaction on Control System Technology (Since 2013), and the IEEE Transaction on Control of System Networks (since 2013). He held the presidency of the European Control Association (EUCA) for the period 2013-2015, and served at the IEEE Board of Governors of the Control System Society 2011-2014. He held the ERC Advanced-Grant 2015 Scale-FreeBack for the period 2016-2021. He is IEEE-Fellow of the IEEE Control System Society and IFAC-Fellow.